



DeActs: genetically encoded tools for perturbing the actin cytoskeleton in single cells

Martin Harterink^{1,7}, Marta Esteves da Silva^{1,7}, Lena Will¹, Julia Turan², Adiljan Ibrahim², Alexander E Lang³, Eljo Y van Battum⁴, R Jeroen Pasterkamp⁴ , Lukas C Kapitein¹, Dmitri Kudryashov⁵, Ben A Barres², Casper C Hoogenraad¹ & J Bradley Zuchero^{2,6} 

The actin cytoskeleton is essential for many fundamental biological processes, but tools for directly manipulating actin dynamics are limited to cell-permeable drugs that preclude single-cell perturbations. Here we describe DeActs, genetically encoded actin-modifying polypeptides, which effectively induce actin disassembly in eukaryotic cells. We demonstrate that DeActs are universal tools for studying the actin cytoskeleton in single cells in culture, tissues, and multicellular organisms including various neurodevelopmental model systems.

Studying the role of the actin cytoskeleton is important for understanding many cell biological processes such as motility and cellular morphogenesis. Perturbation of the actin cytoskeleton is typically achieved using cell-permeable drugs, such as latrunculin or cytochalasin, to promote actin disassembly^{1,2}. However, these pharmacological approaches do not allow for cell-type-specific perturbation and therefore cannot be used to manipulate a subset of cells within complex multicellular model systems. Neuronal development is one example where the role of actin dynamics has been debated³, in part because of the lack of proper tools to manipulate actin in single neurons in culture, tissues, or multicellular organisms. The ideal tool to manipulate the actin cytoskeleton would (i) trigger disassembly of actin filaments in a manner similar to that of latrunculin; (ii) directly interact with actin, rather than inducing cytoskeletal changes indirectly through upstream signaling pathways; (iii) be genetically encoded and not rely on

the addition of ectopic cofactors⁴; and (iv) allow cellular visualization (e.g., as a GFP fusion). Since actin is one of the most highly conserved proteins throughout eukaryotes, this tool would also be broadly applicable in different experimental model systems.

To develop genetic tools that directly target the actin cytoskeleton (disassembly-promoting, encodable actin tools, DeActs), we transiently transfected HeLa cells with candidate peptides (**Fig. 1a** and **Supplementary Fig. 1**) in order to screen both endogenous actin-binding domains that constitutively interact with actin and bacterial toxins that directly modify actin. Gelsolin segment 1 (GS1) is an ~120-amino-acid domain that sequesters actin monomers *in vitro* but lacks both the severing activity and calcium sensitivity of full-length gelsolin^{5,6}. In contrast to the expression of GFP alone, a GFP-GS1 fusion (DeAct-GS1) disrupted actin filaments when expressed in primary rat embryonic fibroblasts and HeLa cells (**Fig. 1b** and **Supplementary Fig. 1**). Actin is a common target of pathogenic bacteria, and numerous species produce toxins that are specific to actin and either covalently modify it or bind it directly⁷. *Salmonella enterica* SpvB is an ADP-ribosyltransferase that ADP-ribosylates actin monomers on a conserved arginine (**Supplementary Fig. 2**) to render them unable to polymerize⁸, leading to net disassembly of all dynamic actin filaments. A GFP fusion with the mono(ADP-ribosyl)transferase domain (DeAct-SpvB) caused complete loss of detectable actin filaments in cells (**Fig. 1b**). As expected, disrupting actin with both DeAct constructs caused defects in cellular actin filament levels and distribution (**Fig. 1c–e**), cell morphology, proliferation, and focal adhesions (**Supplementary Fig. 3**). Furthermore, live imaging revealed that DeActs caused profound defects in cell motility and loss of filopodia dynamics (**Fig. 1f**, **Supplementary Fig. 3**, and **Supplementary Video 1**). In all cases DeAct-SpvB caused more dramatic effects, which is consistent with DeAct-SpvB being an enzyme, while DeAct-GS1 bound stoichiometrically to actin⁵ and thus requires higher expression to induce actin disassembly. Consistently, cell motility was only inhibited at high expression of DeAct-GS1 (**Fig. 1f** and **Supplementary Video 2**), whereas low levels of DeAct-SpvB expression were sufficient to cause efficient actin disassembly (**Fig. 1d**) and inhibit cell motility (**Fig. 1f** and **Supplementary Fig. 3**). To look more closely at the dose dependence of DeAct-GS1, we made use of the observation that *in vitro* differentiated rat oligodendrocyte cells (OLs) do not require an intact actin cytoskeleton to maintain a flattened cell morphology⁹. Expressing DeAct-GS1 in these cells under control of a mature OL promoter¹⁰ induced a dose-dependent loss of actin filaments without causing cell retraction (**Fig. 1g** and **Supplementary Fig. 3**). Finally, to allow inducible DeAct expression

¹Cell Biology, Department of Biology, Faculty of Science, Utrecht University, Utrecht, the Netherlands. ²Department of Neurobiology, Stanford University School of Medicine, Stanford, California, USA. ³Institute for Experimental and Clinical Pharmacology and Toxicology, Albert-Ludwigs University of Freiburg, Freiburg, Germany. ⁴Department of Translational Neuroscience, Brain Center Rudolf Magnus, University Medical Center Utrecht, Utrecht, the Netherlands. ⁵Department of Chemistry and Biochemistry, The Ohio State University, Columbus, Ohio, USA. ⁶Department of Neurosurgery, Stanford University School of Medicine, Stanford, California, USA. ⁷These authors contributed equally to this work. Correspondence should be addressed to C.C.H. (c.hoogenraad@uu.nl) or J.B.Z. (zuchero@stanford.edu).

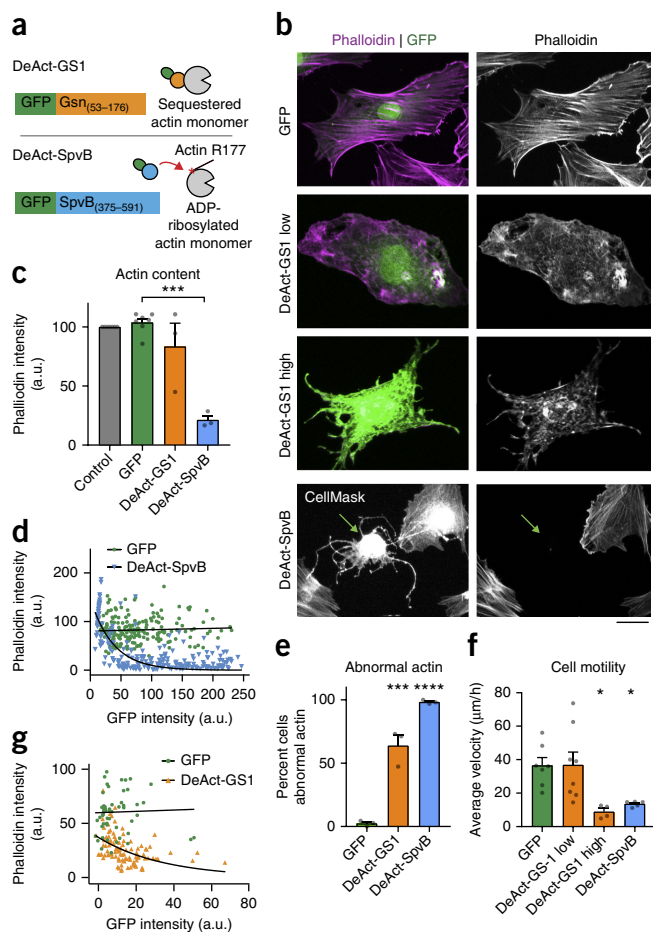


Figure 1 | Construction and characterization of DeActs. **(a)** Schematic of DeAct constructs and mechanism of action. **(b)** Expression of DeActs in rat embryonic fibroblasts, visualized with GFP and Alexa Fluor 594-phalloidin. CellMask Blue was used to reveal full cell morphology upon DeAct-SpvB expression. Scale bar, 20 μm . Representative micrographs from $N = 4$ independent experiments. Arrow points to cell expressing DeAct-SpvB. **(c–e)** Quantification of DeAct effect on actin in rat embryonic fibroblasts showing **(c)** average phalloidin intensities ($N = 7, 7, 3, 3$ independent experiments, left to right), **(d)** phalloidin intensity relative to the DeAct-SpvB level ($n = 207$ GFP or 240 DeAct-SpvB cells), and **(e)** percent of cells with abnormal actin filament distribution ($N = 3$ independent experiments; see **Supplementary Methods**). a.u., arbitrary units. **(f)** Velocities of single-cell motility of rat embryonic fibroblasts transfected with DeActs or GFP control (see also **Supplementary Video 2**). $n = 7, 8, 4,$ or 5 expressing cells per condition, left to right. **(g)** Oligodendrocyte-specific expression of GFP or DeAct-GS1 in primary rat oligodendrocytes using the OL-specific myelin basic protein promoter, quantifying phalloidin intensity relative to the DeAct-GS1 level (fluorescence intensities not directly comparable to panel **d**). $n = 55$ GFP or 103 DeAct-GS1 cells. Graphs show mean \pm s.e.m. Trend lines in **d** and **g** show nonlinear (exponential) fit; each data point is one cell. Statistical significance, one-way ANOVA followed by Dunnett's multiple comparison test. ****, $P < 0.0001$; ***, $P < 0.001$; *, $P < 0.05$.

we made use of the TetOn-3G system (Clontech), which resulted in rapid DeAct expression, efficient actin disruption, and inhibition of cell motility following addition of doxycycline (**Supplementary Fig. 4**). By adding a constitutively expressed mCherry to the same DNA construct in the opposite direction, we also allowed visualization of transfected cells before induction of DeAct expression (**Supplementary Fig. 5**). To suppress background expression

of SpvB in the absence of doxycycline, we fused a DHFRdd destabilization domain¹¹ to SpvB to attenuate SpvB expression (**Supplementary Fig. 5**). Together, these DeAct constructs represent a toolkit for rapid and tunable perturbation of the actin cytoskeleton in cells and simultaneous visualization of affected cells.

We next tested whether DeActs could be used to study the role of actin dynamics in other cellular model systems, such as developing neurons in culture. Primary hippocampal neurons expressing DeAct-GS1 or DeAct-SpvB revealed a robust cell-specific decrease in actin filaments in the axonal growth cone, similar to the decrease that occurs in latrunculin-treated neurons (**Fig. 2a–c**). Growth cone morphology was severely altered with DeAct expression or after latrunculin treatment, with a marked shift from fan- or torpedo-like shape (exploratory and elongating growth cones) to bulb and collapsed shape (stationary or eliminating growth cones)¹² (**Fig. 2a,d**). Whereas in control conditions more than 40% of axonal tips were dynamic, subsequent treatment with latrunculin markedly decreased the number of dynamic tips as expected (**Fig. 2e, Supplementary Fig. 6, and Supplementary Video 3**). Consistently, DeAct expression inhibited axonal growth cone dynamics to a similar extent as did latrunculin (**Fig. 2e and Supplementary Video 3**). Thus, DeActs disrupt the actin cytoskeleton in a cell-specific manner and cause neuronal morphology defects.

A major advantage of genetically encoded DeActs is that they can be used in multicellular organisms where cytoskeletal drugs may have broader effects and/or are more difficult to administer. The first *in vivo* system we used was the developing embryonic mouse neocortex, where newly born neurons polarize and migrate from the ventricular zone toward the cortical plate¹³. We electroporated CMV-promoter-driven DeAct DNA constructs into the brains (motor cortices) of E14.5 mouse embryos *in utero* to target neural precursor cells, then allowed them to develop for 3 d before euthanizing and analyzing cortical migration. In control animals, GFP-positive neurons migrated efficiently to the upper layers of the cortical plate (**Fig. 2f–h**). In contrast, expression of DeAct-GS1 led to a marked decrease in the number of neurons that reached the upper cortical layers, although no clear morphological differences were observed (**Supplementary Fig. 6**). Consistent with our culture studies, neurons expressing DeAct-SpvB failed to become bipolar and did not migrate toward the cortical plate, but instead accumulated in the subventricular zone (**Fig. 2f–h**). Thus, DeActs cause strong developmental defects during neuronal migration *in vivo*.

As a second *in vivo* model we used the nematode *Caenorhabditis elegans*, for which conventional drugs are hard to use on account of this organism's impermeable exoskeleton. The PVD sensory neuron possesses a stereotyped morphology with two highly branched dendrites (anterior and posterior) and an axon that extends first ventrally and then anteriorly into the ventral nerve cord (**Fig. 3a**). We first found that the moesin-based actin marker moeABD¹⁴ was enriched in the many dendritic side branches (**Fig. 3b**). We expressed DeActs using a specific PVD neuron promoter that is activated early during neurite extension¹⁵. Consistent with a role for actin assembly, PVD-neuron-specific DeAct expression led to severe loss of dendrite branching (**Fig. 3b–d**). In addition to branching, primary neurite outgrowth was largely blocked upon DeAct-SpvB expression or high expression of DeAct-GS1

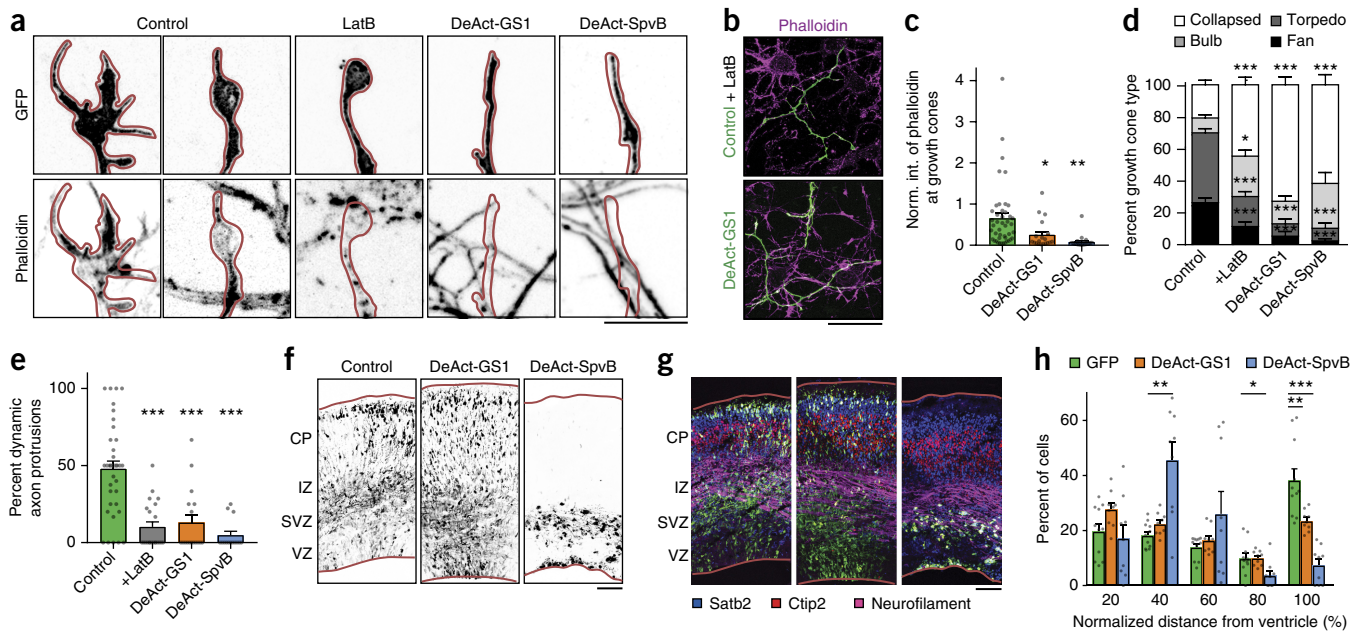


Figure 2 | DeActs markedly affect growth cones and neuronal migration. **(a)** Growth cones of DIV4 rat embryonic hippocampal neurons expressing MARCKS-eGFP ± latrunculin B (LatB) or DeAct-GS1 or DeAct-SpvB and stained with Alexa Fluor 568-phalloidin to visualize actin filaments. Scale bar, 10 μ m. **(b)** Overview of actin filament staining (magenta) in neuronal cultures expressing MARCKS-eGFP and treated with LatB (affects the whole culture) or expressing DeAct-GS1 (cell specific). Scale bar, 40 μ m. **(c)** Quantification of actin filament intensity (int.) in growth cones normalized (norm.) to untransfected neighboring neurons; LatB affects all growth cones and therefore cannot be included ($N = 4, 2, 2$ independent experiments, $n = 44, 19, 22$ neurons, left to right). **(d)** Quantification of growth cone morphology upon MARCKS-eGFP or DeAct expression compared to that of LatB ($N = 4, 2, 2, 2$ independent experiments, $n = 44, 23, 19, 22$ neurons, left to right). **(e)** Dynamics of axonal branches are lost after addition of LatB or in neurons expressing DeAct constructs. ($N = 4, 2, 2, 2$ independent experiments; $n = 37, 22, 17, 14$ neurons, left to right). See also **Supplementary Figure 6** and **Supplementary Video 3**. **(f,g)** Cortical neuronal migration after *in utero* electroporation with GFP (control), DeAct-GS1, or DeAct-SpvB. **(f)** Same slice as **g** combined with immunostaining against Satb2 (cortical layer II-IV), Ctip2 (cortical layer IV-V) and neurofilament (axons in the IZ). CP, Cortical plate; IZ, intermediate zone; SVZ, subventricular zone; VZ, ventricular zone. Scale bar, 100 μ m. **(h)** Quantification of cortical neuronal migration described in **f**. ($N = 3$ embryos from three different litters. $n = 3,412; 2,143; 847$ cells GFP, DeAct-GS1, or DeAct-SpvB). Graphs show mean \pm s.e.m. Statistical significance: one-way ANOVA and Dunnett's multiple comparison post hoc test and Wilcoxon test for paired data. ***, $P < 0.001$; **, $P < 0.01$; *, $P < 0.05$.

(Fig. 3e–g). Thus, DeAct-SpvB led to strong neuronal phenotypes *in vivo*, whereas the severity of the phenotypes induced by DeAct-GS1 was dose dependent.

In conclusion, by repurposing the actin-binding domain of gelsolin (DeAct-GS1) and the actin-modifying enzymatic activity of SpvB (DeAct-SpvB), we created tools that allow for cell-specific perturbation of the actin cytoskeleton both in cultured cells and multicellular *in vivo* model systems. Genetically encodable tools allow for control of actin dynamics using cell-type-specific and inducible promoters, and they open up possibilities for elucidating the role of actin dynamics in fundamental and disease-relevant cellular processes.

METHODS

Methods, including statements of data availability and any associated accession codes and references, are available in the [online version of the paper](#).

Note: Any Supplementary Information and Source Data files are available in the [online version of the paper](#).

ACKNOWLEDGMENTS

We thank C. Bargmann (Rockefeller) for the CX11480 strain; K. Shen (Stanford) for the moesin actin marker; K. Satchell (Northwestern) for MARTX_{VC}; K. Aktories (Albert-Ludwigs University of Freiburg) for TccC3 and C2I; D. Mullins (UCSF) for cofilin(S3A); T. Wandless and L.-c. Chen (Stanford) for DHFRdd;

L. Spector, M. Bennett, E. Vitriol, and M.Z. Lin for helpful discussions; Wormbase; and Stanford Neuroscience Microscopy Service, supported by NIH NS069375. We gratefully acknowledge funding from the Netherlands Organization for Scientific Research (NWO) (NWO-ALW-VENI to M.H., NWO-ALW-VICI to C.C.H., NWO-ALW-VICI to R.J.P.), the European Research Council (ERC Consolidator Grant to C.C.H.), the Deutsche Forschungsgemeinschaft (Germany) project AK6/22-2 (A.E.L.), NIH R01 GM114666 (D.K.), the National Multiple Sclerosis Society (J.B.Z. and B.A.B.), NIH R01 EY10257 (B.A.B.), and the Dr. Miriam and Sheldon G. Adelson Medical Research Foundation (B.A.B.). M.E.d.S. is supported by Fundação para a Ciência e Tecnologia (FCT, Portugal; grant SFRH/BD/68642/2010). J.B.Z. is a Career Transition Award Fellow of the National Multiple Sclerosis Society.

AUTHOR CONTRIBUTIONS

M.H., M.E.d.S., C.C.H., D.K., and J.B.Z. conceived the project. M.H., M.E.d.S., L.W., J.T., A.I., E.Y.v.B., R.J.P., L.C.K., C.C.H., and J.B.Z. planned and/or executed experiments. A.E.L., D.K., and B.A.B. contributed essential reagents and expertise. M.H., M.E.d.S., C.C.H., and J.B.Z. wrote the paper with input from all authors. C.C.H. and J.B.Z. supervised all aspects of the work.

COMPETING FINANCIAL INTERESTS

The authors declare no competing financial interests.

Reprints and permissions information is available online at <http://www.nature.com/reprints/index.html>. Publisher's note: Springer Nature remains neutral with regard to jurisdictional claims in published maps and institutional affiliations.

1. Spector, I., Shochet, N.R., Kashman, Y. & Groweiss, A. *Science* **219**, 493–495 (1983).

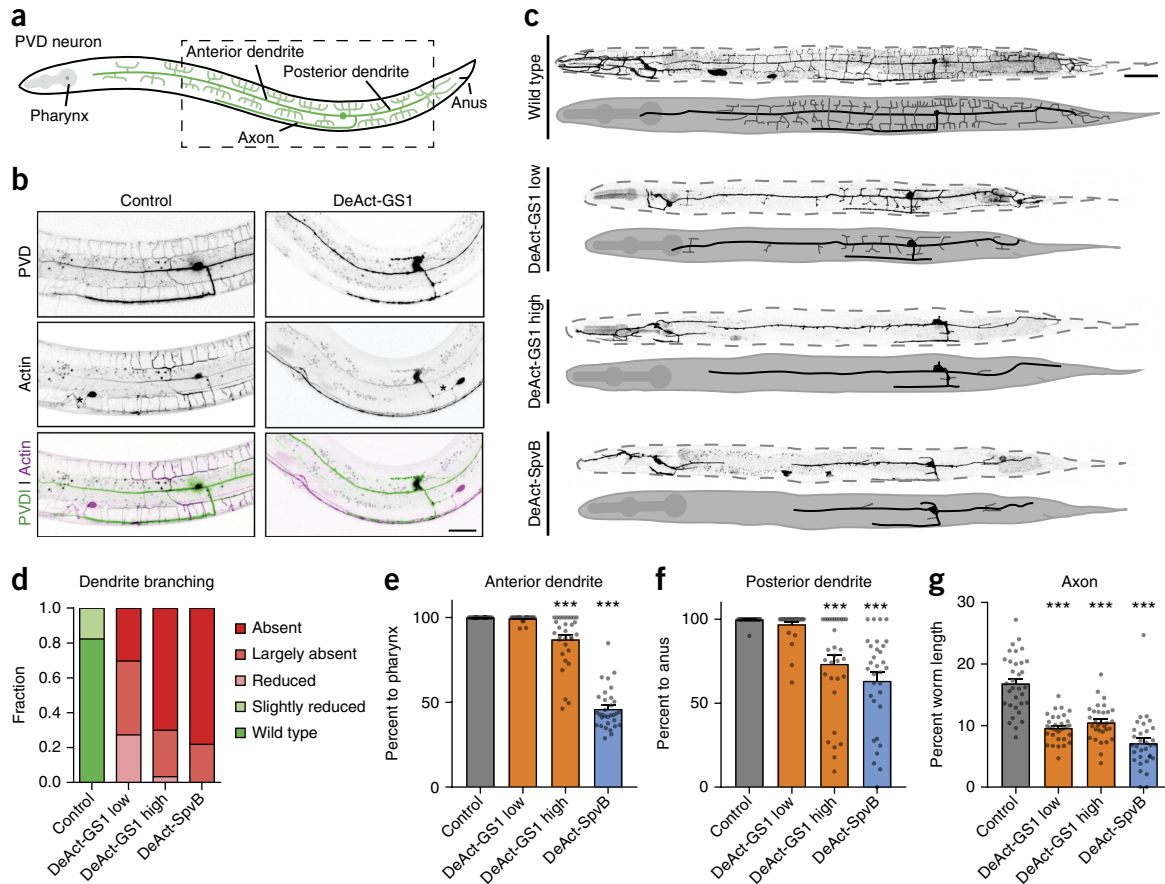


Figure 3 | DeActs efficiently inhibit PVD neuron development in *C. elegans*. (a) Schematic representation of the *C. elegans* highly branched PVD neuron. (b) Coexpression of the moesin/ABD actin marker with GFP (control) or DeAct-GS1 in the PVD neuron. Other neurons expressing the actin marker are marked by *. Scale bar, 20 μm . (c) Representative images and schematic representation of the PVD neuron morphology upon cell-specific DeAct expression. Scale bar, 50 μm . (d–g) Quantification of the DeAct-induced branching defects (d) and primary neurite outgrowth defects (e, f, g). Controls are siblings which lost the DeAct constructs. $N = 34$ for controls, and $N = 32$ for DeAct animals (for DeAct-GS1 64 animals were analyzed and split in low- and high-DeAct-expressing animals). Graphs show mean \pm s.e.m. Statistical significance: one-way ANOVA and Dunnett's multiple comparison *post hoc* test. Micrographs are representative; ***, $P < 0.001$.

- MacLean-Fletcher, S. & Pollard, T.D. *Cell* **20**, 329–341 (1980).
- Vitriol, E.A. & Zheng, J.Q. *Neuron* **73**, 1068–1081 (2012).
- Wu, Y.I. *et al.* *Nature* **461**, 104–108 (2009).
- Way, M., Pope, B., Gooch, J., Hawkins, M. & Weeds, A.G. *EMBO J.* **9**, 4103–4109 (1990).
- McLaughlin, P.J., Gooch, J.T., Mannherz, H.G. & Weeds, A.G. *Nature* **364**, 685–692 (1993).
- Aktories, K., Lang, A.E., Schwan, C. & Mannherz, H.G. *FEBS J.* **278**, 4526–4543 (2011).
- Margarit, S.M., Davidson, W., Frego, L. & Stebbins, C.E. *Structure* **14**, 1219–1229 (2006).
- Zuchero, J.B. *et al.* *Dev. Cell* **34**, 152–167 (2015).
- Gow, A., Friedrich, V.L. Jr. & Lazzarini, R.A. *J. Cell Biol.* **119**, 605–616 (1992).
- Iwamoto, M., Björklund, T., Lundberg, C., Kirik, D. & Wandless, T.J. *Chem. Biol.* **17**, 981–988 (2010).
- van der Vaart, B. *et al.* *Dev. Cell* **27**, 145–160 (2013).
- Barnes, A.P. & Polleux, F. *Annu. Rev. Neurosci.* **32**, 347–381 (2009).
- Chia, P.H., Patel, M.R. & Shen, K. *Nat. Neurosci.* **15**, 234–242 (2012).
- Maniar, T.A. *et al.* *Nat. Neurosci.* **15**, 48–56 (2011).

ONLINE METHODS

Ethics statement. All animal experiments were performed in compliance with the guidelines for the welfare of experimental animals issued by the Government of the Netherlands. All animal experiments were approved by the Animal Ethical Review Committee (DEC) of Utrecht University or were approved by Stanford University's Administrative Panel on Laboratory Animal Care.

Molecular biology and design of DeActs. We used published biochemical data to determine the minimal actin-binding or actin-modifying domains of gelsolin (gelsolin segment 1, GS1)^{5,6,16,17}, *Salmonella enterica* SpvB (mono(ADP-ribosyl) transferase domain)^{8,18,19}, *Vibrio cholerae* MARTX_{VC} (actin-crosslinking domain)^{20,21}, *Salmonella* SipA (actin-crosslinking minimal domain)²², *Photobacterium luminescens* TccC3 (mono(ADP-ribosyl)transferase domain)²³, and *Clostridium botulinum* C2I (mono(ADP-ribosyl)transferase domain)^{24,25}. Despite extensive biochemical data on the mechanisms, specificity, and minimal functional domains of these peptides^{5–8,16–19}, they have not previously been developed as cell biological tools. DNA sequences encoding candidate peptides were cloned into pEGFP-C1 (Clontech) by standard procedures. To create constitutively active cofilin (GFP-P2A-cofilin(S3A))²⁶, we first inserted DNA encoding a P2A self-cleavable peptide into the multicloning site of pEGFP-C1, then we inserted DNA encoding full-length human cofilin(S3A) (kind gift of D. Mullins, UCSF) in frame on the C-terminal side. In the case of DeAct-GS1 and DeAct-SpvB, we truncated proteins within regions predicted to be disordered²⁷.

The following mammalian expression plasmids have been previously described: tagRFP-paxillin²⁸, pGW2-MARCKS-eGFP²⁹, pSuper vector³⁰, pSactin-GFP³¹; *Escherichia coli* dihydrofolate reductase destabilization domain (DHFRdd) with R12Y, G67S, Y100I mutations¹¹ was a gift of T. Wandless and L.-c. Chen (Stanford). pGW2-MARCKS-TagRFP-T was generated by introducing Tag-RFP-T to GW2-MARCKS by PCR strategy. For the *in utero* experiments, DNA encoding DeAct-GS1 and DeAct-SpvB was cloned into the pGW2-GFP vector. For the *C. elegans* experiments the *Pdes-2::mKate2::GS1* and *Pdes-2::mKate2::SpvB* were cloned using multisite Gateway cloning. The *des-2* promoter sequence was based on Maniar *et al.*¹⁵ and cloned into pDONR4-1, the mKate2 sequence (kind gift from H. Bringmann³², Max Planck Institute for Biophysical Chemistry) was cloned into pDONR221, and the DeAct-GS1 or DeAct-SpvB sequences were cloned into pDONR2-3. pKN146 was used as destination vector, which is the pCFJ201 vector supplemented with the *unc-54* UTR (kind gift from H.C. Korswagen, Hubrecht Institute). The cytoplasmic mKate2 was cloned into the pCFJ150 (ref. 33) using the pCM1.36 *tbb-2* UTR (Addgene #17249). All constructs were validated by sequencing. Gelsolin and SpvB sequences used for in DeAct constructs can be found in **Supplementary Data 1**.

Cell culture experiments. HeLa cells (American Type Culture Collection) were cultured in DMEM medium (Life Technologies) supplemented with 10% FBS, 2 mM L-glutamine, nonessential amino acids, and penicillin–streptomycin (all from Gibco) at 37 °C with 5% CO₂. We used cells from ATCC for <5 passages so did not authenticate or test for mycoplasma contamination in house. HeLa Tet-On 3G stable cell line (Clontech cat. no. 631186) were

cultured in the same media, but with Tet System Approved FCS that is guaranteed to have no contaminating tet/dox (Clontech). Expression from the TetON promoter was induced with doxycycline (1–100 ng/mL as noted; Sigma cat. no. D9891). Primary rat embryonic fibroblasts (REFs) were isolated as previously described³⁴ and plated in the same growth media. Briefly, we surgically isolated limbs from E13–E14.5 mixed-sex Sprague Dawley (Charles Rivers) rat embryos, dissociated cells mechanically and with trypsin, then allowed REFs to proliferate in growth media for at least three passages. For transfection, cells were seeded onto glass coverslips and allowed to adhere for 1 d, then transfected using XtremeGENE HP DNA Transfection Reagent (Roche) or Fugene (Roche) according to the manufacturer's protocol, or they were treated with latrunculin A (EMD Millipore) to induce actin disassembly. OPCs were purified from enzymatically dissociated, mixed-sex P7–P8 Sprague Dawley (Charles Rivers) rat brains by immunopanning and grown in serum-free defined medium as previously described³⁵. PDGF (10 ng/ml, PeproTech) and NT-3 (1 ng/ml, PeproTech) were added to the media to induce OPC proliferation. OPCs were transfected as previously described³⁵ using a Lonza/Amara nucleofector kit, with 2–3 × 10⁶ OPCs per transfection then differentiated into mature OLs by removal of PDGF and NT-3 and addition of thyroid hormone (triiodothyronine, T3; 40 ng/ml; Sigma) as described³⁵. We used the myelin basic protein promoter (MBPp)¹⁰ for expression of DeActs in mature OLs.

Cells were fixed in 4% formaldehyde (prepared from paraformaldehyde) for 15 min, permeabilized with 0.1% Triton X-100 for 3 min, then blocked in 3% BSA in PBS. Native GFP fluorescence was visualized to detect DeAct expression. Cells were stained with Alexa Fluor 594-phalloidin (Invitrogen) to visualize actin filaments, DAPI to visualize nuclei, HCS CellMask Blue (Invitrogen) to reveal cellular morphology, or they were immunostained for myelin basic protein (MBP) to detect oligodendrocytes (Abcam cat. no. ab7349, used at 1:100). Cells were visualized by epifluorescence using a Zeiss Axio Imager M1 and Axiovision software, most frequently with a 20× 0.8 NA Plan Apo objective or by confocal using an LSM510 scan head on an Axio Observer Z1 with a 63× 1.4 NA objective (all of the above, Carl Zeiss Microscopy). Identical illumination and acquisition conditions were used for each experiment. Confocal images of HeLa cells for focal adhesion quantification were acquired using LSM700 (Zeiss) with a 40×/1.30 Oil DIC objective using 488 nm and 555 nm laser lines. A total thickness of 5 μm was scanned for each position, and maximum intensity projections were generated for analysis.

Hippocampal neuron cultures, transfections, and drug treatments.

Primary hippocampal cultures were prepared from mixed-sex embryonic day 18 (E18) Wistar rat brains by mechanical and enzymatic dissociation^{36,37}. Cells were plated on coverslips coated with poly-L-lysine (37.5 μg/ml) and laminin (1.25 μg/ml) at a density of 100,000 cells/well. Hippocampal cultures were grown in neurobasal medium (NB) supplemented with B27, 0.5 mM glutamine, 15.6 μM glutamate and penicillin–streptomycin. Hippocampal neurons at DIV2 were transfected using Lipofectamine 2000 (Invitrogen). Briefly, DNA (3.6 μg/well) was mixed with 3 μl Lipofectamine 2000 in 200 μl NB, incubated for 30 min, and then added to the neurons in NB with 0.5 mM glutamine at 37 °C in 5% CO₂ for 45 min to 1 h. Next, neurons

were washed with NB and transferred in the original medium at 37 °C in 5% CO₂ for 36–48 h. Neurons were cotransfected with GFP-tagged MARCKS (control), GS1, or SpvB together with empty pSuper vector. Whenever indicated, 10 μM latrunculin B (Sigma) was added to the neuron cultures and either imaged 1–30 min after addition or fixed after 30 min.

Neuron immunocytochemistry, growth cone morphology, and phalloidin intensity analysis. For immunocytochemistry, neurons were fixed for 10 min with 4% formaldehyde/4% sucrose in PBS at room temperature. After fixation cells were washed three times for 5 min in PBS at room temperature and incubated with Alexa Fluor 568-phalloidin (Life Technologies A12380) for 1 h at room temperature. Neurons were then washed three times for 5 min in PBS at room temperature and subsequently mounted on slides in Vectashield mounting medium (Vector Laboratories). Confocal images were acquired using LSM700 (Zeiss) with a 63×/1.40 Oil or 40×/1.30 Oil DIC objective using 488 nm and 555 nm laser lines. A total thickness of 5 μm was scanned for each position, and maximum intensity projections were generated for analysis. Imaging settings were kept the same when pictures were compared for fluorescence intensity. Growth cone morphology was classified manually, and phalloidin intensity was measured in ImageJ. The entire growth cone areas were considered and normalized to growth cones of untransfected neighboring neurons.

To be able to identify the axon in the live-cell imaging experiments, neuronal cultures were incubated with extracellular Neurofascin-pan mouse primary antibody (NeuroMab, clone number A12/18, 1:100) in conditioned Neurobasal medium for 10 min at 37 °C. After this, neurons were washed three times in warm Neurobasal medium, and anti-mouse Alexa405 antibody (Life Technologies, cat. no. A31553, 1:1,000) in conditioned Neurobasal medium was added for 10 min at 37 °C. Neurons were then washed three times in warm Neurobasal medium and returned to the conditioned medium.

Live-cell imaging microscopy. All imaging was performed in full conditioned medium at 37 °C and 5% CO₂ unless otherwise indicated. For live imaging of REF cell motility, cells were plated on PDL-coated plastic-bottom ImageLock plates (Essen Bioscience) and imaged in an IncuCyte ZOOM Live Cell Imaging System (Essen Bioscience) with 10% CO₂. For wound-healing assays, cells were plated on 5 μg/mL fibronectin, grown until confluent, then mechanically scratch wounded with a sterile p2 pipette tip. Nonadhered cells were washed off with fresh growth media and imaged once per hour. Live-cell imaging of hippocampal neurons was performed by laser confocal spinning disk microscopy using a Nikon Eclipse-Ti (Nikon) microscope with Plan Apo 40× N.A. 1.30 oil objective (Nikon). The microscope is equipped with a motorized stage (ASI; MS-2000), a Perfect Focus System (Nikon), and an incubation chamber (Tokai Hit; INUBG2E-ZILCS); it uses MetaMorph 7.7.6 software (Molecular Devices) to control the camera and all motorized parts. Confocal excitation and detection is achieved using 100 mW Cobolt Calypso 491 nm and 100 mW Cobolt Jive 561 nm lasers and a Yokogawa spinning disk confocal scanning unit (CSU-X1-A1; Yokogawa) equipped with a triple-band dichroic mirror (z405/488/568trans-pc; Chroma) and a filter wheel (CSU-X1-FW-06P-01; Yokogawa) containing BFP (ET-BFP 49021), GFP (ET-GFP (49002)), mCherry (ET-mCherry

(49008)) and mCherry–GFP (ET-mCherry/GFP (59022)) emission filters (all Chroma). Confocal images were acquired with an Evolve 512 EMCCD camera (Photometrics) at a final magnification of 67 nm/pixel, including the additional 2.0× magnification introduced by an additional lens mounted between scanning unit and camera (Edmund Optics). For quantifying single-cell motility of fibroblasts, we first imaged the GFP channel to identify GFP- or DeAct-expressing cells, then we subsequently imaged with phase microscopy to limit phototoxicity until the final frame of the video at 15 min intervals. To classify DeAct-GS1-expressing cells as high or low expressers, we quantified average cellular GFP intensity from initial fluorescence images (background subtracted, ImageJ), and we defined high expressers as those cells with GFP signals above the median value. Cell motility was measured in ImageJ by first aligning images with the StackReg plugin then measuring displacement of the nucleus using the MTrackJ plugin.

Axonal branches were imaged in time lapses of 5 min with 5 s intervals between acquisition and a z-stack stream at every timepoint to guarantee the entire axonal branch complexity was imaged. In control conditions (MARCKS-eGFP), 5 or 6 neurons were first imaged in Neurobasal medium. After that, 10 μM latrunculin B (Sigma) was added to the imaging chamber, and the same cells were imaged from 1 to 30 min. The dynamics of axonal branches were quantified manually using ImageJ.

Time-lapse live-cell imaging of filopodia dynamics in HeLa cells was performed using a TIRF microscope (Nikon Eclipse TE2000E) equipped with an incubation chamber (Tokai Hit; INUG2-ZILCS-H2) mounted on a motorized stage (Prior). Cells were imaged in full medium at 37 °C and 5% CO₂ every 5 s for 5 min using a 100× objective (Apo TIRF 100×/NA 1.49, Nikon) and an Evolve 512 EMCCD camera (Photometrics)³⁸. Excitation was achieved using a 488 nm LuxX488-100 diode laser and a 561 nm Cobolt Jive laser fiber coupled to the Nikon TIRF module. GFP-expressing cells treated with Latrunculin B were first imaged without the drug and then imaged again after 5 to 30 min upon addition of 10 μM of Latrunculin. Quantification of total and dynamic filopodia numbers was performed using ImageJ.

In utero electroporation and immunohistochemistry. Pregnant C57Bl/6 mice at E14.5 were deeply anaesthetized with Isoflurane (induction, 3–4%; surgery, 1.5–2%), injected with 0.05 mg/kg buprenorfinhydrochloride in saline, and hereafter the abdominal cavity was opened under sterile surgical conditions. Uterine horns were exposed, and 1.7 μl DNA mixture containing (pGW2-GFP alone or together with DeAct-GS1 or DeAct-SpvB) dissolved in MilliQ water with 0.05% Fast Green (Sigma) was injected in the lateral ventricles of the embryos using glass micropipettes (Harvard Apparatus) and a PLI-200 Pico-injector (Harvard Apparatus). Brains (motor cortex) were electroporated with gold-plated tweezer electrodes (Fischer Scientific) using an ECM 830 Electro-Square-Porator (Harvard Apparatus) set to three unipolar pulses at 30 V (100 ms interval and pulse length). Embryos were placed back into the abdomen, and abdominal muscles and skin were sutured separately. The mother mice were awakened by releasing them from Isoflurane. Embryos were collected at E17.5, and brains were fixed in 4% formaldehyde and submerged in 30% sucrose. 12 μm coronal brain cryosections were made and were blocked and permeabilized in 10% normal horse serum + 0.2% Triton X-100 in PBS before staining with first antibody

(anti-GFP, MBL-Sanbio cat. no. 598, 1:800; anti-Ctip2, Abcam cat. no. ab18465, 1:1,000; anti-Neurofilament heavy chain, Abcam cat. no. ab72996, 1:500; anti-Satb2, Abcam cat. no. ab51502, 1:20) in blocking solution overnight and fluorescent secondary antibody staining (Alexa Fluor 568-phalloidin, Thermo Fisher, 1:200; Alexa 488 anti-rabbit, Life Technologies, cat. no. A11034, 1:500; Alexa 568 anti-rat, Life Technologies, cat. no. A11077, 1:500; Alexa 647 anti-mouse, Life Technologies, cat. no. A21236, 1:500) and mounting with Vectashield mounting medium (Vectorlabs). Confocal images were acquired using LSM700 (Zeiss) with a 20×/0.8 objective using 405 nm, 488 nm, 555 nm, and 633 nm laser lines. A total thickness of 15 μm in 1 μm steps was scanned for each position, and maximum intensity projections were generated for analysis. To cover the entire brain slice, four images were taken side by side; and image stitching was performed using ZEN 2011 Software. Nine mixed-sex mouse embryos from three litters were analyzed.

Caenorhabditis elegans strains, transgenes, and imaging. Strains were cultured using standard conditions³⁹ at 15 °C and imaged at room temperature at the L4 or young adult stage. For the PVD morphology experiments the DeAct-GS1 and DeAct-SpvB constructs were injected in either NC1686 (*wdIs51*), which expressed GFP in the PVD, or in STR58 (*hrtIs3[Pdes-2::myristoylGFP;unc-122::DsRed]*), which is an integrant of CX11480 (*kyEx3017*)¹⁵, generating: STR198 *hrtIs3;hrtEx52[Pdes-2::mKate2::GS1(20ng/μl);Pmyo-2::tdTom]*, STR199 *wdIs51;hrtEx53[Pdes-2::mKate2::GS1(4ng/μl);Pmyo-2::tdTom]*, STR200 *hrtIs3;hrtEx54[Pdes-2::mKate2::SpvB(4ng/μl);Pmyo-2::tdTom]*. The actin marker strains were generated using a construct expressing the moesin actin-binding domain (kind gift from K. Shen, Stanford¹⁴), generating: STR213 *hrtEx60[Punc-86::GFP::moeABD;Pdes-2::mKate2;Pmyo-2::tdTom]*; STR232 *hrtEx68[Pdes-2::mKate2::GS1(20ng/μl);Punc-86::GFP::moeABD;Pmyo-2::tdTom]*. Worms were anesthetized with 10 mM tetramisole, imaged by confocal microscopy and maximum intensity projections of acquired z-stacks (1 μm steps), and straightening of the animal was done using ImageJ software (Universal Imaging Corporation).

Data analysis and statistics. All data acquisition and analysis were performed blinded to the experimental condition. We used nested analysis to first average technical replicates (e.g., three coverslips). In all cases *N* refers to number of independent experiments for cell culture experiments, or number of mice or worms for *in vivo* experiments (while *n* refers to technical replicates). Sample sizes used were similar to those generally employed in the field. Animals were allocated randomly to each experimental group. Data shown are from all animals tested; none were treated as outliers. Micrographs were analyzed using NIH ImageJ and linearly contrast adjusted for display using Adobe Photoshop, with identical settings for each experiment. For quantification of fluorescent and phase micrographs, ROIs were drawn by hand or by thresholding multichannel images using ImageJ (NIH). Mean gray value (average intensity) of each individual channel was measured, and background (outside of cell area) was subtracted

for each micrograph. Qualitative scoring of abnormal actin in cells was performed by an investigator blinded to experimental condition. In our hands untransfected rat embryonic fibroblasts had stereotyped phalloidin staining with similar filament intensities and distribution (e.g., stress fibers and cortical actin). GFP+ cells were considered abnormal if they had dim phalloidin staining or disorganized actin filaments (lacking stress fibers and/or presence of actin filament foci as in latrunculin-treated cells), excluding mitotic cells. Data were analyzed and plotted using Excel (Microsoft) and Prism (GraphPad Software). Unless otherwise stated, error bars are SEM, and *P* values were calculated using Student's *t*-test for single comparisons or ANOVA followed by Dunnett's multiple comparison test, assuming equal variance.

Data availability statement. The data that support the findings of this study are available from the corresponding authors upon request. The following plasmids have been deposited at Addgene: pCMV-DeAct-GS1 (Addgene plasmid 89445), pCMV-DeAct-SpvB (Addgene plasmid 89446), pTetON-EGFP (Addgene plasmid 89453), pTetON-DeAct-GS1 (Addgene plasmid 89454), and pTetON-DHFRdd-SpvB+CMV-mCherry (Addgene plasmid 89463). Other plasmids are available upon request.

- Way, M., Pope, B. & Weeds, A.G. *J. Cell Biol.* **116**, 1135–1143 (1992).
- Finidori, J., Friederich, E., Kwiatkowski, D.J. & Louvard, D. *J. Cell Biol.* **116**, 1145–1155 (1992).
- Tezcan-Merdol, D. *et al. Mol. Microbiol.* **39**, 606–619 (2001).
- Hochmann, H., Pust, S., von Figura, G., Aktories, K. & Barth, H. *Biochemistry* **45**, 1271–1277 (2006).
- Sheahan, K.-L., Cordero, C.L. & Satchell, K.J.F. *Proc. Natl. Acad. Sci. USA* **101**, 9798–9803 (2004).
- Kudryashov, D.S. *et al. Proc. Natl. Acad. Sci. USA* **105**, 18537–18542 (2008).
- Lilic, M. *et al. Science* **301**, 1918–1921 (2003).
- Lang, A.E. *et al. Science* **327**, 1139–1142 (2010).
- Vandekerckhove, J., Schering, B., Bärmann, M. & Aktories, K. *J. Biol. Chem.* **263**, 696–700 (1988).
- Schleberger, C., Hochmann, H., Barth, H., Aktories, K. & Schulz, G.E. *J. Mol. Biol.* **364**, 705–715 (2006).
- Agnew, B.J., Minamide, L.S. & Bamburg, J.R. *J. Biol. Chem.* **270**, 17582–17587 (1995).
- Li, X., Romero, P., Rani, M., Dunker, A.K. & Obradovic, Z. *Genome Inform. Ser. Workshop Genome Inform.* **10**, 30–40 (1999).
- Bouchet, B.P. *et al. eLife* **5**, e18124 (2016).
- Schätzle, P. *et al. J. Physiol. (Lond.)* **589**, 4353–4364 (2011).
- Brummelkamp, T.R., Bernards, R. & Agami, R. *Science* **296**, 550–553 (2002).
- Kapitein, L.C. *et al. Biophys. J.* **99**, 2143–2152 (2010).
- Redemann, S. *et al. Nat. Methods* **8**, 250–252 (2011).
- Frøkjær-Jensen, C. *et al. Nat. Genet.* **40**, 1375–1383 (2008).
- Vierbuchen, T. *et al. Nature* **463**, 1035–1041 (2010).
- Dugas, J.C., Tai, Y.C., Speed, T.P., Ngai, J. & Barres, B.A. *J. Neurosci.* **26**, 10967–10983 (2006).
- Goslin, K. & Banker, G. *J. Cell Biol.* **108**, 1507–1516 (1989).
- Kapitein, L.C., Yau, K.W. & Hoogenraad, C.C. *Methods Cell Biol.* **97**, 111–132 (2010).
- Kapitein, L.C. *et al. Curr. Biol.* **23**, 828–834 (2013).
- Brenner, S. *Genetics* **77**, 71–94 (1974).